

**PERFORMANCE ANALYSIS OF SUPERCONDUCTING WAVEGUIDES
AND REFLECTOR ANTENNAS IN RADIO TELESCOPES**

ONG SING SEAN

**A project report submitted in partial fulfilment of the
requirements for the award of the degree of
Bachelor of Engineering (Hons) Electronic Engineering**

**Faculty of Engineering and Green Technology
Universiti Tunku Abdul Rahman**

May 2016

DECLARATION

I hereby declare that this project report is based on my original work except for citations and quotations which have been duly acknowledged. I also declare that it has not been previously and concurrently submitted for any other degree or award at UTAR or other institutions.

Signature : _____

Name : Ong Sing Sean

ID No. : 11AGB03403

Date : 4th April 2016

APPROVAL FOR SUBMISSION

I certify that this project report entitled **“PERFORMANCE ANALYSIS OF SUPERCONDUCTING WAVEGUIDES AND REFLECTOR ANTENNAS IN RADIO TELESCOPES”** was prepared by **ONG SING SEAN** has met the required standard for submission in partial fulfilment of the requirements for the award of Bachelor of Engineering (Hons) Electronic Engineering at Universiti Tunku Abdul Rahman.

Approved by,

Signature : _____

Supervisor: Dr. Yeap Kim Ho

Date : _____

The copyright of this report belongs to the author under the terms of the copyright Act 1987 as qualified by Intellectual Property Policy of Universiti Tunku Abdul Rahman. Due acknowledgement shall always be made of the use of any material contained in, or derived from, this report.

© 2016, Ong Sing Sean. All right reserved.

Specially dedicated to
my beloved father and mother, for their everlasting love and support.

ACKNOWLEDGEMENTS

I would like to thank everyone who had contributed to the successful completion of this project. I would like to express my gratitude to my research supervisor, Dr. Yeap Kim Ho for his invaluable advice, guidance and his enormous patience throughout the development of the research.

In addition, I would also like to express my gratitude to my loving parent and friends who had helped and given me encouragement when I needed them. Without their everlasting love and support, I would not achieve my goal today. Their words and encouragemets are always in my mind.

Lastly, I would like to thank my fellow friends and course mates in the Electronic Engineering programme at UTAR for their support. They gave me strength to fulfil my dream. We have been through four years together and we will appreciate those memories forever.

**PERFORMANCE ANALYSIS OF SUPERCONDUCTING WAVEGUIDES
AND REFLECTOR ANTENNAS IN RADIO TELESCOPES**

ABSTRACT

In this project, we perform an analysis on two components at the front end of a radio telescope, which are the reflector antenna and waveguide. Waveguide characterization must be implemented in a radio telescope to improve the performance of transmission from the horn to the receiver circuits. The design configuration of the ALMA Cassegrain antenna was applied to detect signal with lower frequency such as 10 GHz. The radiation pattern at the subreflector shows reasonably good results. This proves that the ALMA telescope is able to perform well even with a lower frequency applied onto it. Superconducting waveguides are also proposed to minimize the loss of signal in the transmission system of a radio telescope. Here, Noguchi-Naruse-Sekimoto's formulation was applied in a superconducting circular waveguides to analyse the loss of signals. The results show that a superconducting waveguide exhibits low but finite loss below the gap frequency. The loss, however, turns out to be higher than normal conducting waveguide when the frequency is above the gap frequency. The higher loss can be attributed to the higher surface resistance and field penetration for superconducting waveguides operating above the gap frequency.

TABLE OF CONTENTS

DECLARATION	ii
APPROVAL FOR SUBMISSION	iii
ACKNOWLEDGEMENTS	vi
ABSTRACT	vii
TABLE OF CONTENTS	viii
LIST OF TABLES	x
LIST OF FIGURES	xi
LIST OF SYMBOLS / ABBREVIATIONS	xiii
LIST OF APPENDICES	xv

CHAPTER

1	INTRODUCTION	1
	1.1 Scientific Motivation	1
	1.2 Background Study	2
	1.3 Aims and Objectives	3
2	LITERATURE REVIEW	4
	2.1 Introduction	4
	2.2 Reflector Antenna	6
	2.3 Waveguides	7
	2.3.1 Circular waveguide	9
3	REFLECTOR ANTENNAS	10
	3.1 Introduction	10
	3.2 Methodology	12

	3.2.1	FEKO	13
	3.2.2	Configuration Data of Antenna	15
	3.3	Results and Discussion	18
4		SUPERCONDUCTING WAVEGUIDES	21
	4.1	Introduction	21
	4.2	Superconductivity	22
	4.3	Theories	23
	4.3.1	Meissner Effect	23
	4.3.2	Type-II Superconductor	25
	4.3.3	Cooper Pairs	26
	4.3.4	Mattis-Bardeen's Formulation	27
	4.3.5	Noguchi-Naruse-Sekimoto Formulation	29
	4.3.6	TE and TM Modes of Circular Waveguides	30
	4.4	Results and Discussion	32
	4.4.1	Skin Depth	36
	4.4.2	Surface Resistance	38
5		CONCLUSION AND RECOMMENDATIONS	40
	5.1	Conclusion	40
	5.2	Recommendation	41
	5.2.1	Superconducting Waveguides	41
	5.2.2	Reflector Antennas	42
		REFERENCES	43
		APPENDICES	47

LIST OF TABLES

TABLE	TITLE	PAGE
3.1	Configuration data of Cassegrain antenna (Tham & Withington, 2003)	15

LIST OF FIGURES

FIGURE	TITLE	PAGE
2.1	Block diagram of a radio telescope (Yeap et al., 2013)	5
2.2	Configuration of a Cassegrain Antenna	6
2.3	Uniform plane wave (Raju, 2006)	7
2.4	Wave propagation of TE and TM waves.	8
2.5	Various circular waveguide modes (Marcuvitz, 1951)	9
3.1	Process flows of antenna's simulation using FEKO	12
3.2	The work flows in FEKO	14
3.3	Optical configuration of ALMA Cassegrain antenna (Tham & Withington, 2003)	14
3.4	Meshed model of a corrugated horn	16
3.5	Measurement of primary reflector and focal length in FEKO	16
3.6	Measurement of secondary reflector and centre hole in FEKO	17
3.7	Vertical cut V-N plane and vertical cut U-N plane	17
3.8	Radiation pattern of full hybrid coupling method	18
3.9	Zoom in view of the radiation pattern by using full hybrid coupling method	19
3.10	Radiation pattern of decoupling method	20
3.11	Zoom in view of radiation pattern by using decoupling method	20

4.1	Characteristic of Superconductor	22
4.2	Meissner Effect	24
4.3	Magnetic field of type-II superconductor	25
4.4	The correlation of a Cooper pair (Baquero, 2005)	26
4.5	A circular waveguide	30
4.6	Attenuation before cutoff frequency, f_c	32
4.7	Attenuation from cutoff to millimeter wave frequencies	33
4.8	Attenuation from cutoff to THz frequencies	34
4.9	Attenuation in a superconducting Nb waveguide at the vicinity of gap frequency	35
4.10	Comparisons between the skin depth of Nb in superconducting and normal states, with f below f_g	36
4.11	Comparisons between the skin depth of Nb in superconducting and normal states, with $f = 0$ GHz to $f = 2000$ GHz	37
4.12	The surface resistance of Nb in both normal and superconducting state	38

LIST OF SYMBOLS / ABBREVIATIONS

E_F	Fermi energy
f_g	Gap frequency
f_c	Cutoff frequency
T	Temperature
TE	Transverse Electric
TM	Transverse Magnetic
Nb	Niobium
Δ	Energy gap at Fermi surface
σ_n	Normal conductivity
σ	Complex conductivity
μ_ω	Permeability of the wall material of waveguides
ϵ_ω	Permittivity of the wall material of waveguides
E	Electric field
H	Magnetic field
\hbar	Reduced Planck's constant
ω	Angular frequency
γ_E	Euler's constant
μ_0	Permeability of free space
μ	Permeability of wall material
ϵ_0	Permittivity of free space
k_x	Transverse wavenumber in the x direction
k_y	Transverse wavenumber in the y direction
k_z	Propagation constant
ϕ_x	Penetration factor in the x direction
a	Height of waveguide
J_n	Bessel function
N	Number of half waves

n_n	Number density of quasiparticles
λ_L	London penetration depth
R_s	Surface resistance
δ	Skin depth

LIST OF APPENDICES

APPENDIX	TITLE	PAGE
A	Gantt chart below shows the work progress of the project.	47

CHAPTER 1

INTRODUCTION

1.1 Scientific Motivation

Among the electromagnetic spectrum, microwave and optical signals are well developed for the radio telescope in the study of cosmology nowadays. However, the technology of terahertz signal is still at its infancy period. In recent years, the frequency band of terahertz electromagnetic region has caught the attention of the researchers in many fields such as analysis in medical and chemical field due to its ability to peer through dust and opaque object (Hosako et al., 2007). Therefore, the research in the terahertz region is very attractive since it represents the new era of technology. Furthermore, the devices and methods that utilize this technology were expected to lead to a revolution of technology (Leal-Sevillano et al., 2011).

To detect the terahertz signals, submillimeter radio telescopes with superconducting heterodyne detector mounted onto it are implemented. The ALMA telescope is one of the devices that operates at the frequency band within the terahertz region. ALMA is a group of huge radio telescopes which contains an array of 66 12-meters and 7-metres Cassegrain type reflector antennas, which have the frequency range from 31 GHz to 950 GHz (Tham et al., 2007). In addition, waveguide in the terahertz region also plays an important role due to its usefulness in many circuits and systems. In fact, waveguide characterization must be implemented in a radio telescope system to improve its performance (Akalın et al., 2006).

1.2 Background Study

The electromagnetic spectrum is categorized into different radiation types from the lowest frequency radio wave to the highest gamma ray. Most of them are invisible to human's naked eyes. Signal at the submillimeter region originates from the coldest and most distant places in the universe, which is far away from our planet Earth. Therefore, these extraterrestrial signals are extremely weak.

To enhance the detection of the weak terahertz signal, a well-developed waveguide is required to be mounted onto the superconductor-insulator-superconductor (SIS) heterodyne receiver (Yeap et al., 2015). Metallic conducting materials, such as gold and copper, act as good conductors in between the frequency band of microwave and millimeter wave. However, these materials may exhibit high attenuation at terahertz frequencies.

In order to minimize signal loss, superconducting materials such as Niobium (Nb) have been implemented in receiver circuits. Superconductors have been found to exhibit much lower loss in comparison with conventional conductors. Yeap et. al. (2015) have performed a theoretical study on superconducting rectangular waveguides. In their study, analysis based on Mattis-Bardeen's (MB) and Noguchi-Naruse-Sekimoto's (NNS') theory were performed. From their results, it was shown that NNS' theory gave a more realistic description on the behaviour of superconductors. Analysis on superconducting circular waveguide based on MB's theory have been found in the literature (Yeap et al., 2011; Yassin et al., 2003). However, none has been found based on the NNS' theory so far. In this project, NNS' theory is incorporated into the study of superconducting circular waveguide. Like Yeap et. al. (2015), the attenuation found using NNS' theory is compared with that found using MB's theory.

Cassegrain antennas have been applied in the ALMA telescope for the detection of THz signal. Here, the applicability of the ALMA antenna at lower frequency is investigated. A Cassegrain reflector antenna with the same design configuration on the ALMA telescope is applied to detect signal with 10 GHz. As shown in the subsequent section, the antenna shows reasonably good results at 10 GHz as well.

1.3 Aims and Objectives

The objectives of the thesis are shown as follows.

- i) To study the loss in superconducting waveguides.
- ii) To simulate the performance of reflector antennas in radio telescopes.

CHAPTER 2

LITERATURE REVIEW

2.1 Introduction

Terahertz (THz) region is the frequency band of the electromagnetic spectrum which is located in between microwave and infrared frequency (300GHz to 3000GHz). Signal at the submillimeter region originates from the coldest and most distant places in the universe, which is far away from our planet Earth. Therefore, submillimeter observation can easily peer through the star formation in the galaxy and will extend our knowledge into the denser regions during star formation. With the advancement in terahertz technology, many new and useful applications beneficial to mankind are expected to be developed (Michael, 2005).

A radio telescope usually employs a paraboloid shape reflector antenna which receives radio wave. In contrast to an optical telescope, radio telescope normally does not observe through visible light but detect frequencies or radiations emitted by the objects or sources in the universe. ALMA is a ground based which is used to detect signals at the millimeter and submillimeter wavelengths.

In a radio telescope system, it consists of several main structures which enables it to receive terahertz signals from outer space. In our project, two main parts among the radio telescope's structure are discussed. The first one is the reflector antenna. The function of the reflector antenna is to receive the electromagnetic waves which travel in outer space. Cassegrain reflector system is well known in practical approach because it allows minimum feeder length to the terminal equipment. The second one is waveguide. Waveguide acts as a feeder system to an antenna because it transmits electromagnetic wave in a waveguide structure. Figure 2.1 shows the block diagram of a radio telescope.

In millimeter or submillimeter receiver system, waveguides play an important role for the propagation of wave. It is used to channel signals to the superconductor-insulator-superconductor (SIS) heterodyne receiver. Signals from cosmic sources are usually extremely weak. Hence, it is important to minimize attenuation during detection. Superconductors are known to be excellent materials with very low loss. Here, analysis of superconducting circular waveguides is performed. The analysis based on Mattis-Bardeen's and Noguchi-Naruse-Sekimoto's formulations are performed here.

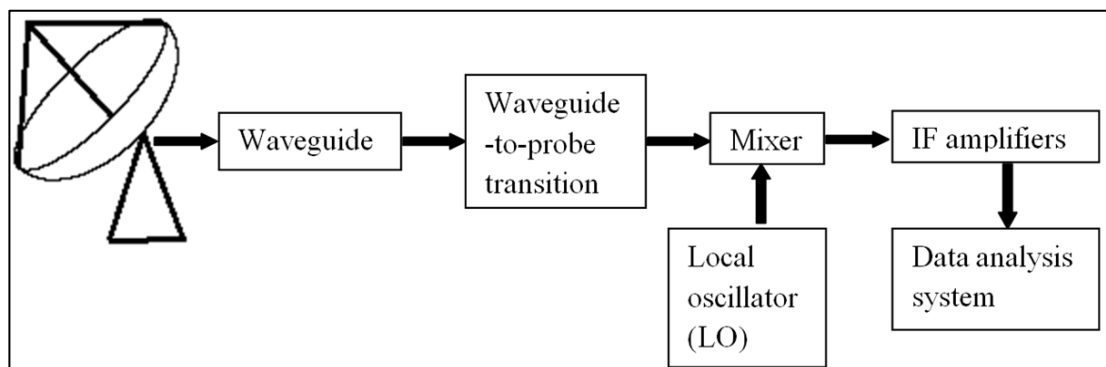


Figure 2.1: Block diagram of a radio telescope (Yeap et al., 2013)

2.2 Reflector Antenna

The function of the Cassegrain antenna is to enhance the performance of huge ground based microwave reflector antennas which are used to perform satellite tracking and communication. Cassegrain antenna is a system which consists of a main and a secondary reflector. The main reflector is paraboloid in shape and the secondary reflector is hyperboloid in shape. The main reflector must be designed larger than the secondary reflector in order to achieve the desired collimation characteristics (Balanis, 2005).

There are many advantages of using a Cassegrain antenna. First of all, it can be used to locate the feed horn in a suitable place. The blockage caused by the huge amplifier and long transmission line can be avoided. Thus, the unwanted signals and noise are removed without the presence of blockage. Moreover, the reduction of the minor lobe radiation and spillover will increase the accuracy of the result. Furthermore, Cassegrain antennas are capable of obtaining an equivalent focal length which is much greater than the physical length. Last but not least, it has the capability of scanning and broadening the beam by relocating the reflector surfaces. Figure 2.2 below shows the configuration of a Cassegrain antenna.

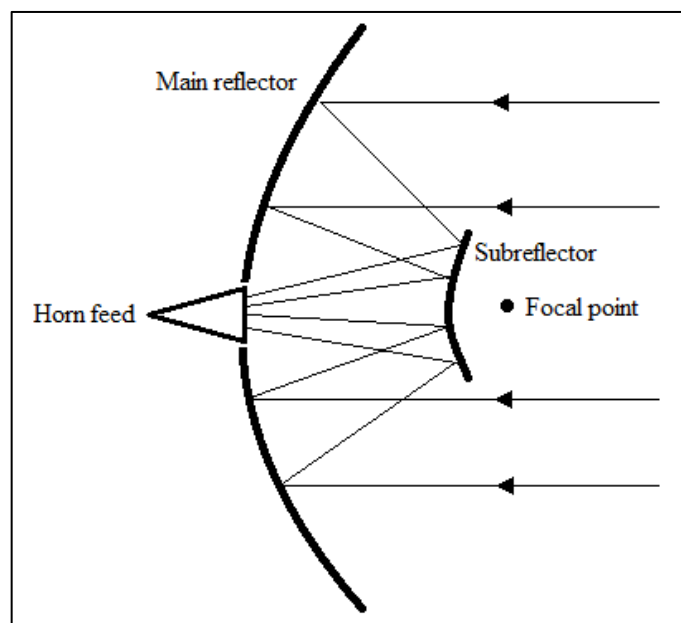


Figure 2.2: Configuration of a Cassegrain Antenna

2.3 Waveguides

A waveguide is a type of transmission line which transmits electrical signals and waves. Generally, a waveguide is a hollow metallic tube which transmits electrical signal. It acts as a guide for the electromagnetic waves to flow through (Bakshi & Bakshi, 2008). There are many other transmission lines such as open-wire lines, cable and coaxial lines. However, these transmission lines may exhibit high losses in a very high frequency signal such as microwave. Thus, they are not suitable to be utilized in high frequency band such as terahertz frequency application. Waveguides conduct electrical signals at lower loss at higher frequency among all other transmission lines. Thus, it is practical for a waveguide to be implemented in a terahertz frequency application.

Waves propagating in free space exhibit the characteristic of uniform plane waves. An electromagnetic wave that propagates toward the direction of x-plane is said to be a uniform plane wave if its electric and magnetic fields are orthogonal to each other and the fields do not have x-component, that is $E_x = 0$ and $H_x = 0$, where E is the electric field vector and H is the magnetic field vector. E and H are always perpendicular to each other as seen in Figure 2.3 (Raju, 2006).

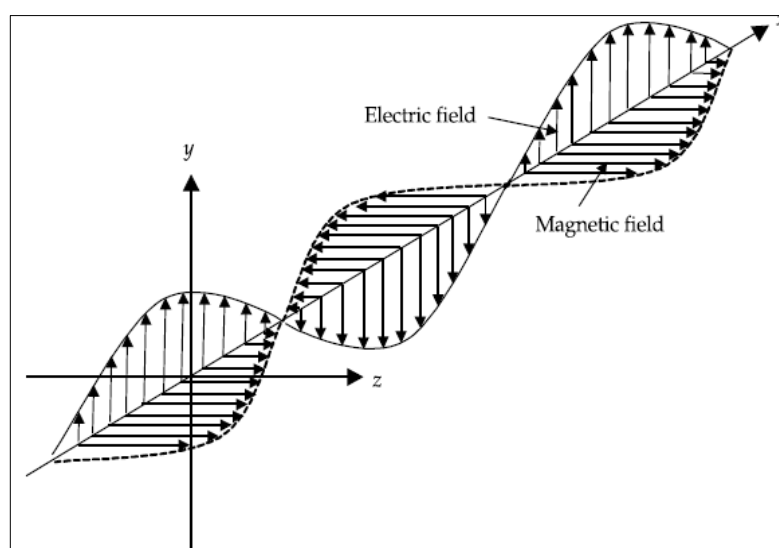


Figure 2.3: Uniform plane wave (Raju, 2006)

However, for waveguide, the electromagnetic waves are guided along the structure of the waveguide. Since electromagnetic waves do not propagate in free space, they are not uniform plane wave and their propagation characteristics are described in term of the Transverse Magnetic (TM) and Transverse Electric (TE) waves. Consequently, waveguide consists of two modes which is the TM mode and the TE mode. TM wave implies that there is no component of magnetic field toward the direction of propagation, $H_z = 0$; TE wave carries the meaning that there is no electric field component in the direction of propagation, $E_z = 0$. Figure 2.4 shows the wave propagation of electric field E , and magnetic field, H of TE and TM waves (Raju, 2006). TEM mode can only exist in structures with two conductors. Hence, waveguides cannot support TEM modes.

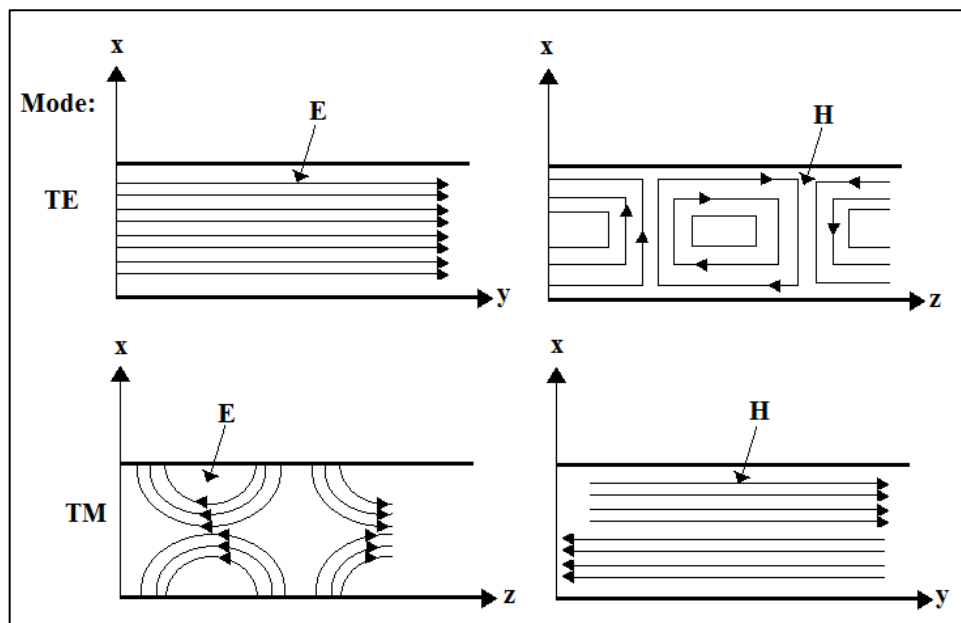


Figure 2.4: Wave propagation of TE and TM waves.

2.3.1 Circular waveguide

A circular waveguide is a wave-guided structure which is circular in shape. Nowadays, circular waveguide is quite popular particularly in the application telecommunication. For example, a research was carried out to investigate the modes and attenuation constants in circular hollow waveguide (Kato & Miyagi, 1992). Figure 2.5 shows some of the circular waveguide modes. The line in the waveguide shows the direction of the fields i.e. the solid lines indicate electric fields, and the dotted lines are magnetic fields.

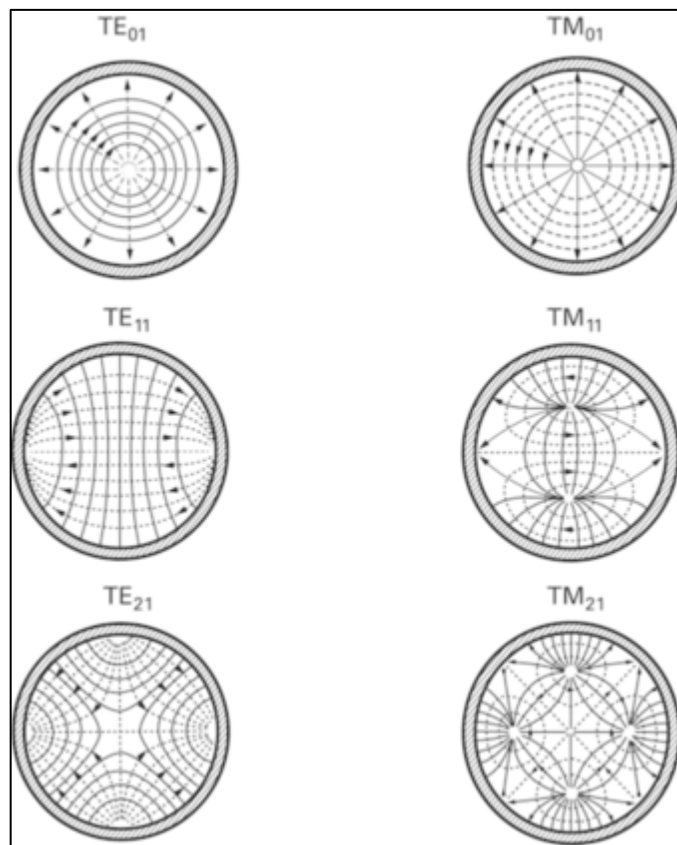


Figure 2.5: Various circular waveguide modes (Marcuvitz, 1951)

CHAPTER 3

REFLECTOR ANTENNAS

3.1 Introduction

To analyse the reflector antenna, we have to assume plane wave field irradiates the antenna's aperture from a far field source. Coupling efficiency is determined at the subreflector. In order to ensure minimum blockage, the diameter of the subreflector is designed to be small. In addition, smaller diameter of the subreflector triggers high truncation of the Gaussian beam field, and thus producing high taper efficiency. However, such design will increase spillover hence the aperture efficiency is reduced (Tham et al., 2007).

The power distribution across the profile of Gaussian beam is as shown in (3.1)

$$\frac{P(r)}{P(0)} = \exp\left(\frac{-2r^2}{w^2}\right) \quad (3.1)$$

where

r = Distance from beam axis

w = Beam waist

The edge taper is defined as the relative power density at a radius $r = r_e$. Equation (3.2) illustrates the function of edge taper (Tham et al., 2007).

$$T_e = -10 \log_{10} \left(\frac{P(r_e)}{P(0)} \right) \quad (3.2)$$

The fractional blockage is the ratio of the radius of subreflector to main reflector, which is $f_b = r_s / r_a$. The energy of the Gaussian beam is not fully intercepted by the secondary reflector. The energy lost is known as spillover. Aperture efficiency is the fractional power coupled from the plane wave to the antenna. It is defined as

$$\begin{aligned} \epsilon_a &= \epsilon_T \times \epsilon_s \\ \epsilon_a &= 2\alpha^{-1} [\exp(-f_b^2 \alpha) - \exp(-\alpha)]^2 \end{aligned} \quad (3.3)$$

where

ϵ_a = Aperture efficiency

ϵ_T = Taper efficiency

ϵ_s = Spillover efficiency

Taper efficiency is shown in equation (3.4), while spillover efficiency is defined in equation (3.5). Spillover efficiency is the fraction of power in the feed illumination of the aperture plane that is intercepted by the antenna aperture (Goldsmith, 1998).

$$\epsilon_T = 2\alpha^{-1} \frac{[\exp(-f_b^2 \alpha) - \exp(-\alpha)]^2}{1 - \exp(-2\alpha)} \quad (3.4)$$

$$\epsilon_s = 1 - \exp(-2\alpha) \quad (3.5)$$

where,

$$\alpha = 0.115T_e$$

f_b = Fractional blockage

The spillover efficiency is maximized for large α , corresponding to a high degree of central concentration of the illumination distribution. Nevertheless, the taper efficiency is maximized for small α , which produces the most consistent illumination over the aperture. Therefore, it yields the highest coupling to a plane wave (Goldsmith, 1998).

3.2 Methodology

The flowchart in Figure 3.1 shows the process in simulating the antenna using FEKO.

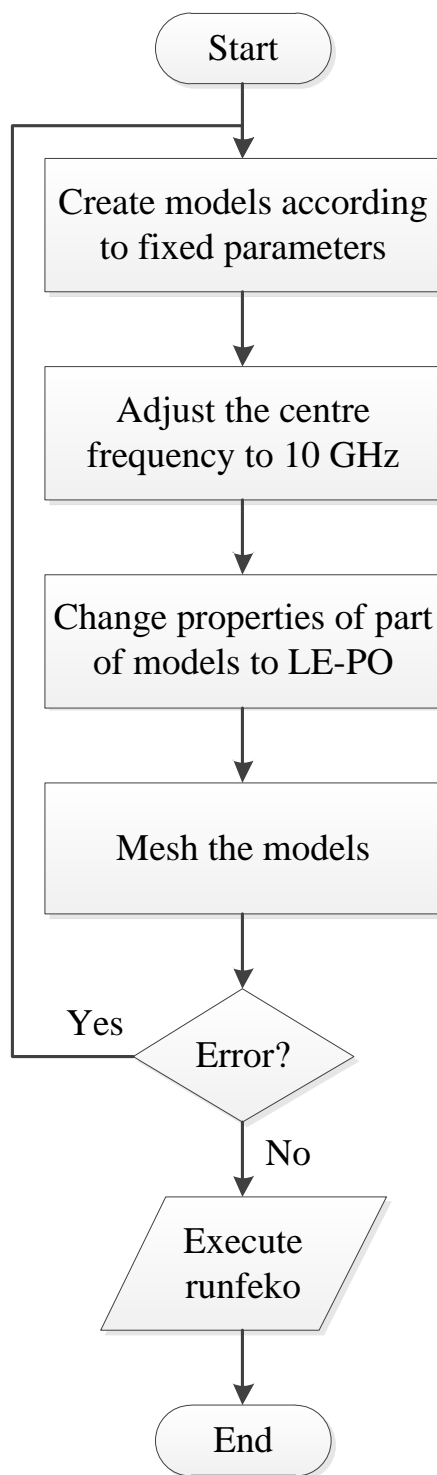


Figure 3.1: Process flows of antenna's simulation using FEKO

3.2.1 FEKO

FEKO is an electromagnetic simulation software tool for electromagnetic field analysis of 3D structure. It offers numerous techniques for the solution of Maxwell's equation. This software enables users to analyse electromagnetic problems encountered in different type of industries. Since FEKO allows the analysis of antenna design, FEKO was chosen to simulate the reflector antenna to observe its characteristic. There are many formulations which enable the analysis of practical antenna problems in FEKO.

The FEKO solver is based on Method of Moments (MoM) which was widespread use in the solution of integral equation formulations of electromagnetic scattering problems. It was the first commercial code to implement the multi-level fast multipole method (MLFMM) for the solution of electrically large problems. The special features of FEKO is multiple solutions and can be hybridized and apply to different parts of model to optimize the solution time and results. In FEKO, the Method of Moments (MoM) can be hybridized with several methods, which is Finite Element Method (FEM), Physical Optics (PO), Geometric Optics (GO), and Uniform Theory of Diffraction (UTD).

Method of Moment (MoM) is an accurate approach of analysing 3D models. However, it can be very time consuming and expensive because it requires a lot of computation power and times. Therefore, traditional MoM analysis is inherently limited to electrically small and moderately large electromagnetic structures. Recently, several current-based hybrid general methods were established and implemented for modeling of three-dimensional (3-D) metallic radiation and scattering structures.

In this project, the results of antenna were categorized into two parts, which is hybrid coupling and decoupling method. Hybrid coupling means the combination of Method of Moments (MoM) and Physical Optics (PO) method while decoupling method carries the meaning in the opposite way.

As we can see in Figure 3.2, the work flows of simulation of an antenna was described in details. In our project, a Cassegrain antenna was created using the ALMA band geometry. Therefore, the structures of the antenna was described in a fixed parameters. However, the frequency supplied was adjusted to 10 GHz as we need to investigate the performance of ALMA telescope in the microwave region frequency instead of terahertz frequency band. The optical configurations of the Cassegrain antenna is shown in Figure 3.3.



Figure 3.2: The work flows in FEKO

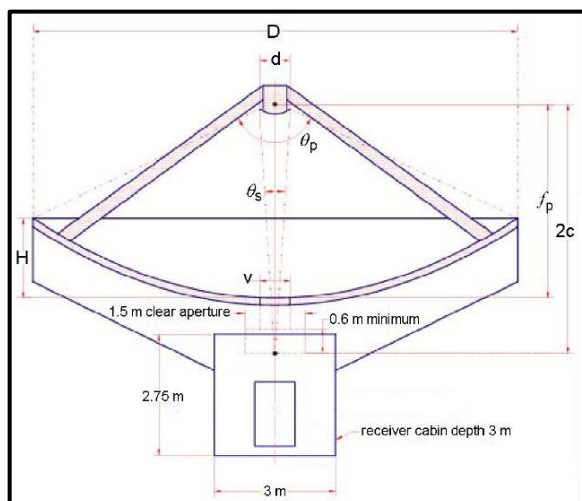


Figure 3.3: Optical configuration of ALMA Cassegrain antenna (Tham & Withington, 2003)

3.2.2 Configuration Data of Antenna

The configuration data for Cassegrain antenna is described in Table 3.1.

Table 3.1: Configuration data of Cassegrain antenna (Tham & Withington, 2003)

Symbol	Description	Data
D	Primary Aperture	12.0m
f_p	Focal Length of Primary	4.8m
	f/D of Primary	0.4
d	Secondary Aperture	0.75m
	Final f/D	8
e	Secondary Eccentricity	1.10526
θ_p	Primary Angle of Illumination	128.02°
θ_s	Secondary Angle of Illumination	7.16°
$2c$	Distance Between Primary and Secondary Foci	6.177m
v	Primary Vertex Hole Clear Aperture	0.75m

After the geometry of the antenna was built using the fixed parameters of ALMA telescope, the centre frequency was adjusted to 10 GHz. Next, the properties of large plate in Cassegrain antenna was changed to solve with special solution using Large Element Physical Optic (LE-PO) method. As we can see in previous research (Hu et al., 2009), a hybrid of Large Element Physical Optic (LE-PO) and Method of Moments (MoM) yields an accurate result instead of using an approach throughout a whole model.

The next step is to mesh the whole structure of the antenna to form a 3D structure of antenna as shown in Figure 3.4. FEKO's automated meshing helps user by configuring frequency, solution method, media properties, curvatures and electrical size of a model and creating a fine, standard or coarse mesh accordingly. After meshing, the antenna's model is ready to perform simulation by executing FEKO solver. In the solver setting, the solver was adjusted to implement the multi-level fast multipole method (MLFMM) to solve the large-size Cassegrain antenna.

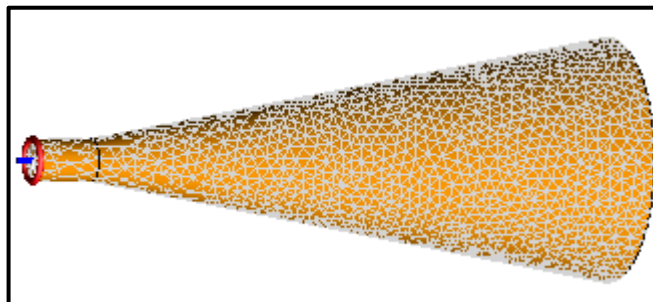


Figure 3.4: Meshed model of a corrugated horn

Figure 3.5 shows a constructed Cassegrain antenna's model according to the fixed parameter of the ALMA telescope. It was supplied with a centre frequency of 10 GHz to simulate its performance in term of gain. The arrow which is pointing upward is the corrugated horn. It is to be noted that the geometry follows the ALMA telescope described in (Tham et al., 2007). As we can see in Figure 3.5, The radius of the primary reflector's radome is 6 m while the focal length of is 4.8 m. Figure 3.6 shows the measurement of the secondary reflector and the centre hole in FEKO. The secondary reflector has a diameter of 0.75 m.

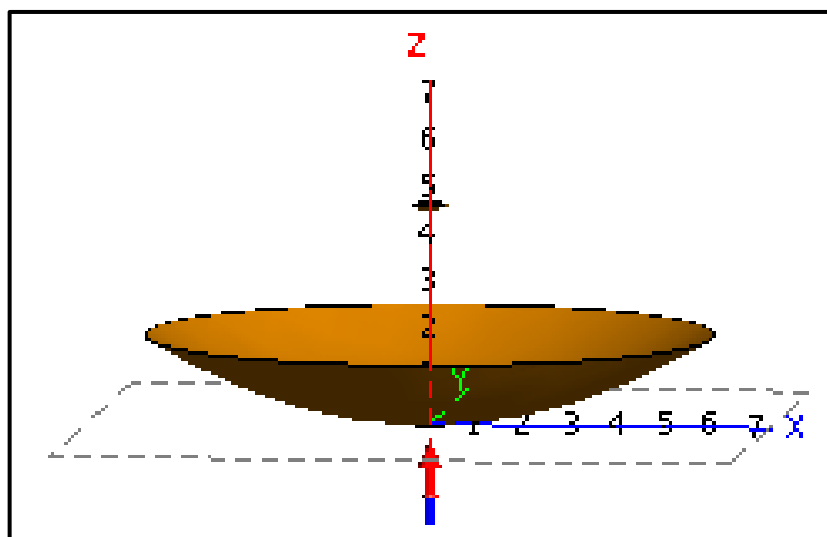


Figure 3.5: Measurement of primary reflector and focal length in FEKO

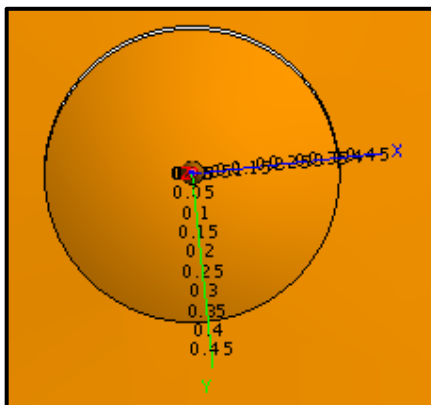


Figure 3.6: Measurement of secondary reflector and centre hole in FEKO

The radiation pattern of the antenna is categorized into four parts, which is far field 1, far field 1 fine, far field 2, and far field 2 fine. As we can see in Figure 3.7. Far field 1 represents the vertical cut in the direction of the V-N plane while far field 2 represents the vertical cut in the direction of the U-N plane.

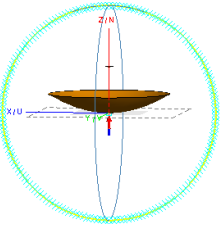
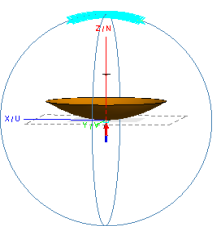
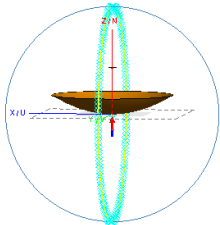
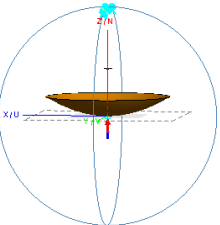
Far field 1	Far field 1 fine
	
Far field 2	Far field 2 fine
	

Figure 3.7: Vertical cut V-N plane and vertical cut U-N plane

3.3 Results and Discussion

As shown in Figure 3.8, an ALMA-structure Cassegrain antenna is simulated using the full hybrid coupling method. In this project, Large-Element Physical Optics (LE-PO) and Method of Moments (MoM) were hybridized to generate a radiation pattern. For instance, LE-PO was implemented in the main reflector of the Cassegrain antenna since the structure of main reflector is very large and requires more computation time. Furthermore, the subreflector was implemented with MoM since the structure is smaller and does not need a longer period of simulation time.

The preliminary result from the shows that the Cassegrain antenna based on the ALMA configuration generates a reasonably good result although it is operating at a lower frequency of 10 GHz. This is because, the side lobes are significantly lower than the main lobe as observed in Figure 3.8. Besides, as observed in Figure 3.9, the main lobe of the radiation pattern is symmetry and it is centered at zero. This fact is very important because it shows that distortion is low. In order to retrieve an image with high resolution, the signal must not be distorted.

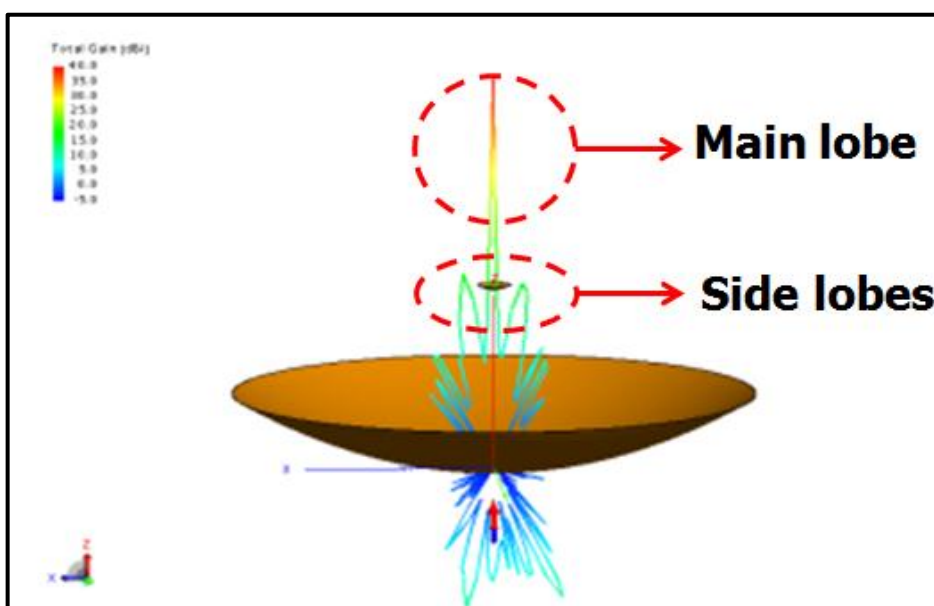


Figure 3.8: Radiation pattern of full hybrid coupling method

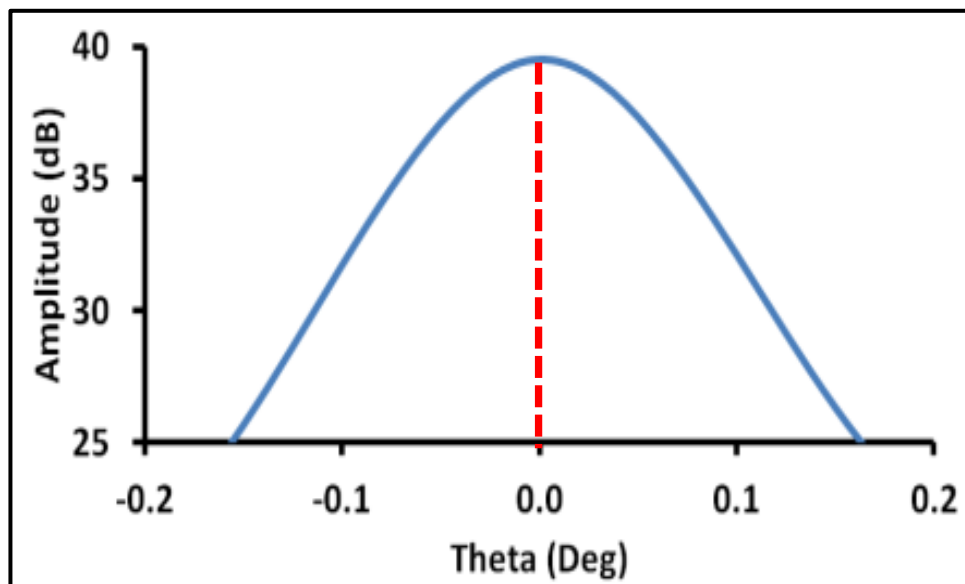


Figure 3.9: Zoom in view of the radiation pattern by using full hybrid coupling method

The Cassegrain antenna with the same structure is simulated using decoupling method. A decoupling method simply means that, the Physical Optics (PO) method and the Method of Moments (MoM) are decoupled from each other. Therefore, only the Method of Moments is used in the simulation.

As can be observed in Figure 3.10, the main lobe and side lobes of the radiation pattern were absent. In fact, the radiation pattern generated was distorted due to the decoupling method applied in the simulation. This will affect the loss of signal when it is transmitting from one point to another. On the other hand, as shown in Figure 3.11, the main lobe of the radiation pattern is not symmetry and it is not centered at zero. Therefore, simulation of Cassegrain antenna does not show good result by applying a decoupling method because there are distortion of signals found in the radiation pattern generated.

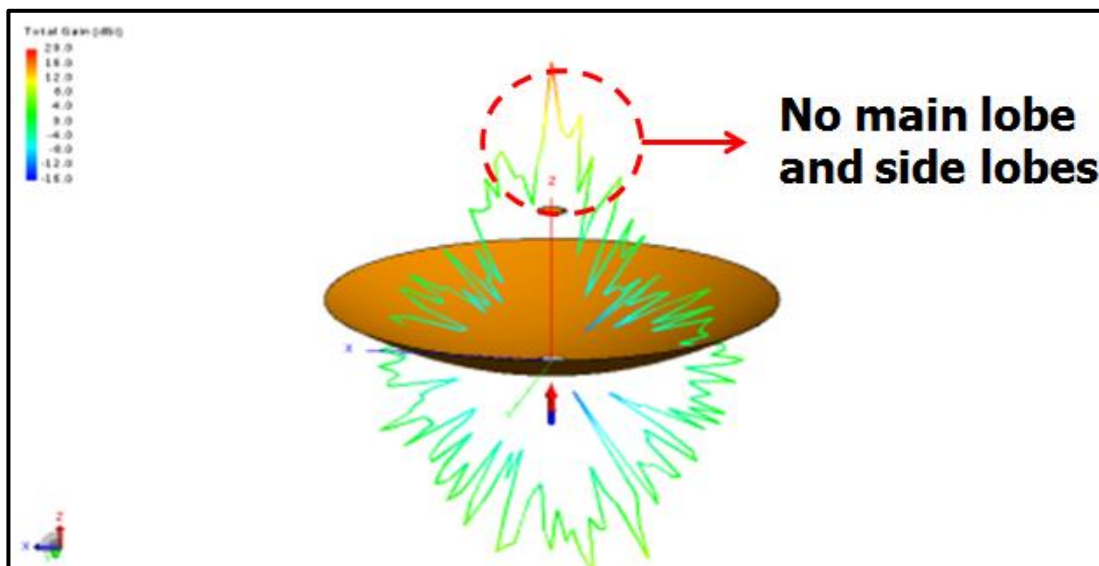


Figure 3.10: Radiation pattern of decoupling method

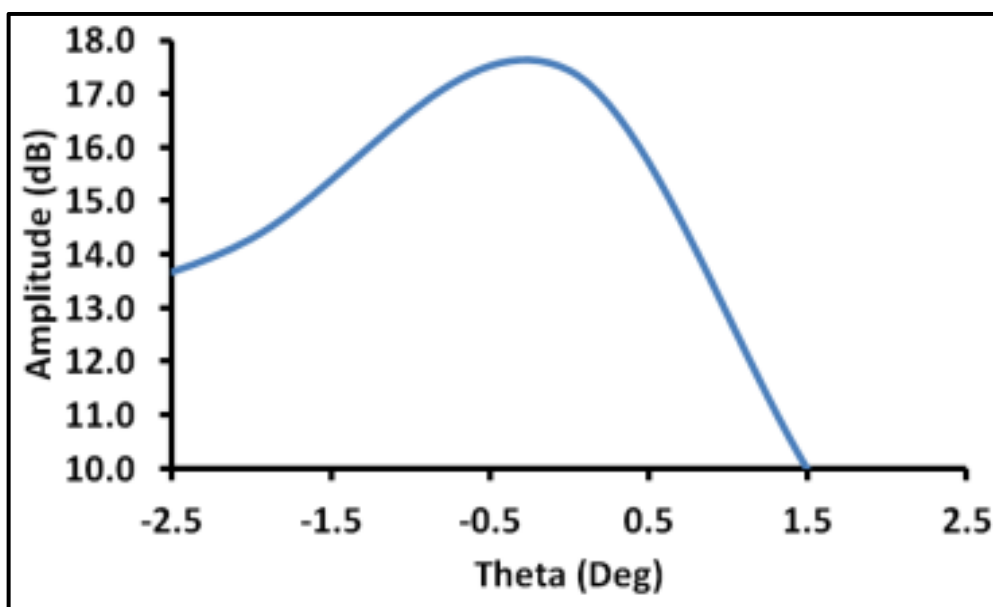


Figure 3.11: Zoom in view of radiation pattern by using decoupling method

From the results, we can conclude that hybrid full coupling of MoM and PO is more accurate than decoupling method in the simulation of Cassegrain antenna. Furthermore, the preliminary result indicates that the Cassegrain antenna using the same design configuration as the ALMA radio telescope may be applicable at 10 GHz.

CHAPTER 4

SUPERCONDUCTING WAVEGUIDES

4.1 Introduction

In order to minimize the loss of signal, superconducting materials such as Niobium (Nb) have been applied in receiver circuit. Rigorous formulation of different methods were carried out to investigate the attenuation in superconducting circular waveguides. The first method is using the Mattis-Bardeen's formulation while the second method is using Noguchi-Naruse-Sekimoto's formulation. The result is obtained by incorporating the complex conductivity equation for superconductors into the characteristic equation developed by Yeap (2011) describe wave propagation in a circular waveguide.

The results are categorized into three parts. The first part is to discuss the relationship of the attenuation and the frequency. The second part is to discuss the skin depth in the waveguide as a function of frequency. Lastly, the third part is to discuss how surface resistance of the material changes when frequency varies.

4.2 Superconductivity

Superconductivity is a phenomenon where a material drops below their critical temperature and conducts electricity without any resistance. Superconductivity was first discovered by H. Kamerlingh Onnes at Leiden in 1911. Superconducting material are called superconductor. However, superconductor is not necessarily a material which possesses metallic characteristic. A heavily doped semiconductor such as Germanium and Silicon can be a superconductor. A good conductor on the other hand may not be a good superconductor too. When the temperature is decreasing, the resistance of a superconductor gradually decreases until it reaches its critical temperature, T_c . The resistance decreases drastically to the point of zero when it reaches its critical temperature, as shown in Figure 4.1.

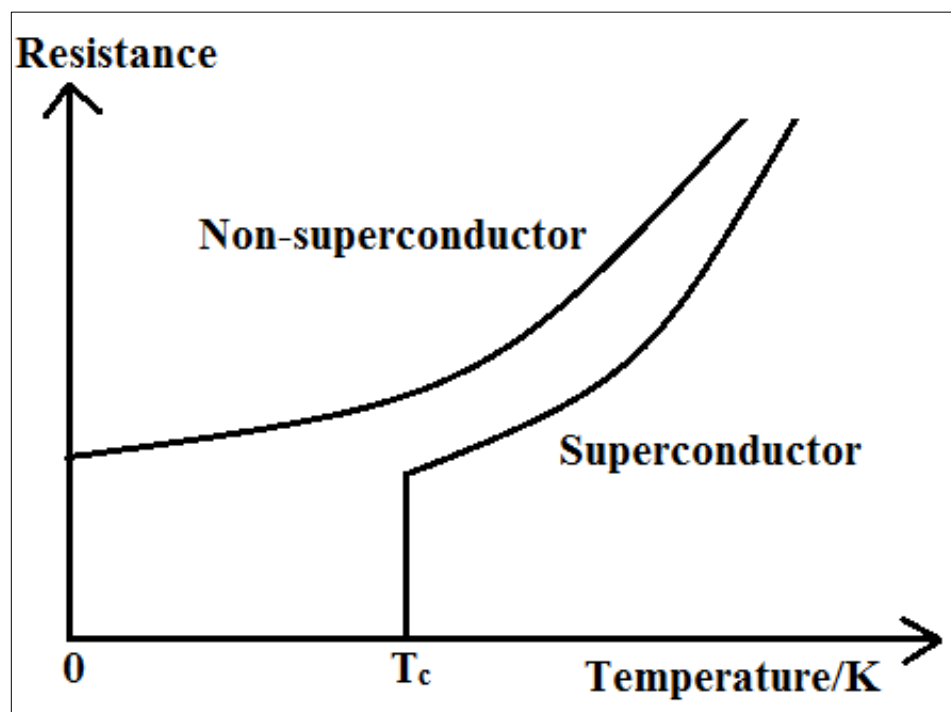


Figure 4.1: Characteristic of Superconductor

Generally, the quality of a superconductor is determined by its critical temperature, T_c . Most of the common superconductors have a very low critical temperature. The highest critical temperature of material is found in a compound called Niobium-Germanium (Nb_3Ge). It was fabricated for the first time in 1973 (Baquero, 2005). Since this compound has a very high critical temperature, it was able to transmit signal faster. Therefore, this compound is applied in the structure of heterodyne receiver to collect the signal of terahertz frequencies. Moreover, there are research which shows that the signal of transmission in a superconductor is much stronger than a normal conductor (John et al., 1988).

4.3 Theories

BCS theory (Bardeen-Cooper-Schrieffer), as its name implies, was proposed by John Bardeen, Leon Cooper, and John Schrieffer. It is assumed that each electron shifts independently in a field determined by the other ions and electrons. As a result, BCS theory states that superconducting phase transition is to schedule the electronic system so that an energy gap is established in the electronic band structures in both sides of the Fermi level. After this theory was introduced, various superconductivity effect such as Meissner effect and zero resistivity were successfully developed (Kopnin, 2009).

4.3.1 Meissner Effect

Meissner effect was discovered by Meissner and Ochsenfeld in 1933. Meissner effect states that when a material drops below its critical temperature, the magnetic field, H tends to be expelled from the interior of the superconductor. Figure 4.2 below shows that Meissner effect occurs when a conductor transitions into a superconductor, it tends to repulse the magnetic flux.

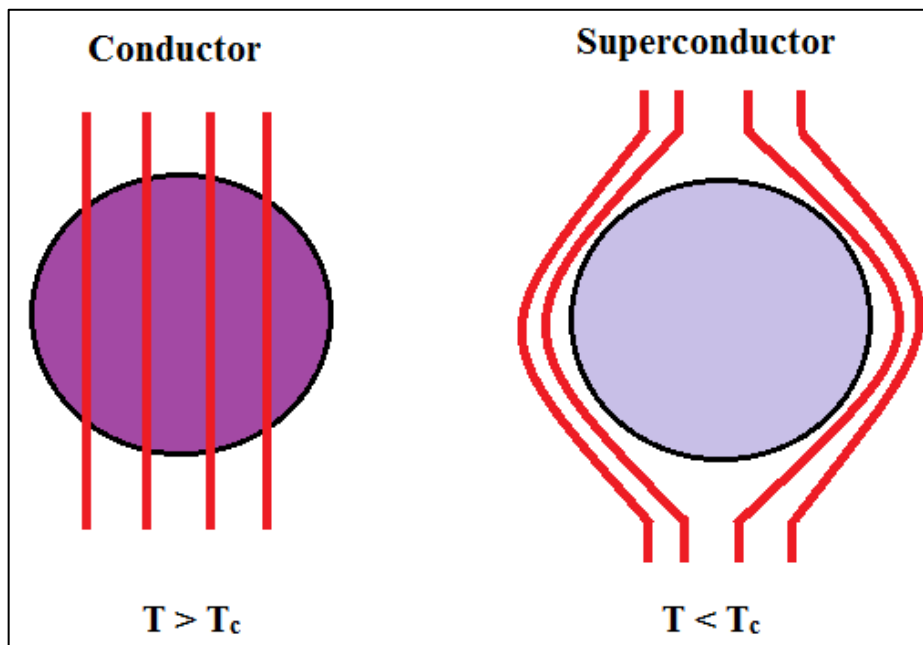


Figure 4.2: Meissner Effect

Recently, it is discovered that the transition temperature changes with the mass of the ionic lattice as in equation (4.1) below

$$\sqrt{M} T_c = \text{constant} \quad (4.1)$$

This phenomenon is also known as the isotope effect. It states that the electron-photon interaction is involved in the transition into the superconducting state. From this theory, we can conclude that superconductors do not possess direct current resistance in normal case. However, they will exhibit resistance in certain circumstances. After years of development in superconductor, it was discovered that superconductor can be categorized into type-I and type-II superconductors. The theory for the characteristic of type-II superconductor was profoundly enhanced by Alexei Alexeyevich Abrikosov, who was awarded the Nobel Prize in Physics in 2003. Generally, a type-I superconductor can exhibit the characteristic of Meissner effect but type-II superconductor does not show such effect.

4.3.2 Type-II Superconductor

For type-II superconductors, they are energetically favourable for a magnetic field, H to partially penetrate a superconductor breaking it up into many superconductor and normal regions as shown in Figure 4.3.

Type-II superconductors can support very large magnetic fields and transmit very high currents. There are some commonly used type-II superconductor material which are widely used in civilian, military and astronomy. They are niobium-tin, and niobium-titanium which are known as the compound of type-II superconductor. In the astronomical aspect, Niobium (Nb) which is a type-II superconductor was implemented in the heterodyne receiver of the radio telescope. These radio telescopes are required to detect weak signal in terahertz region. This can be done by Niobium (Nb) since its characteristic of sustaining large magnetic field and carry high current. Thus, a type-II superconductor is highly recommended to configure in a radio telescope with terahertz technology.

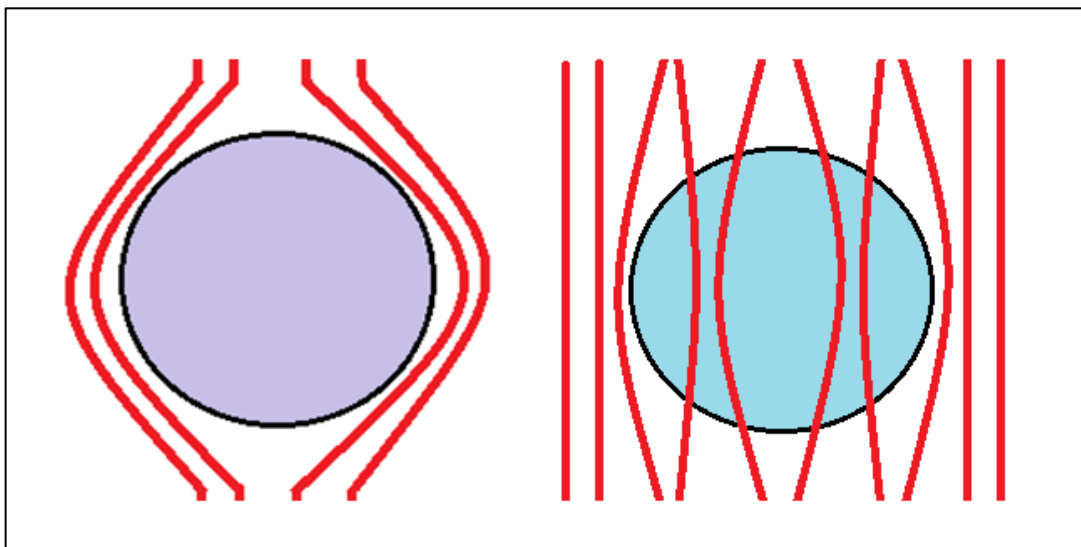


Figure 4.3: Magnetic field of type-II superconductor

4.3.3 Cooper Pairs

In short, superconductivity is the physics of Cooper pairs. A Cooper pair is a bound state of two electrons with energy at the Fermi surface and spin and momentum of opposite sign (Baquero, 2005). Electrons that can pass through the space formed by consistent arrangement of ions will undergo transition of state when it is below its critical temperature, T_c .

Through the process of state transition, Cooper pairs are formed and they exhibit some special characteristic changes which stimulate the growth of new technology. From Figure 4.4, we can observe that an attraction potential for electron 2 is produced by the polarization triggered by electron 1.

In the theory of Cooper pair, a non-interacting Fermi gas at $T = 0$ K is considered so that all of the states increased up to Fermi level. The electron energy ε_k is stated in equation (4.2).

$$\varepsilon_k = \frac{p^2}{2m} = \frac{\hbar^2 k^2}{2m} \quad (4.2)$$

$$k_F = \frac{\sqrt{2m\varepsilon_F}}{\hbar} \quad (4.3)$$

where

k_F = Fermi momentum

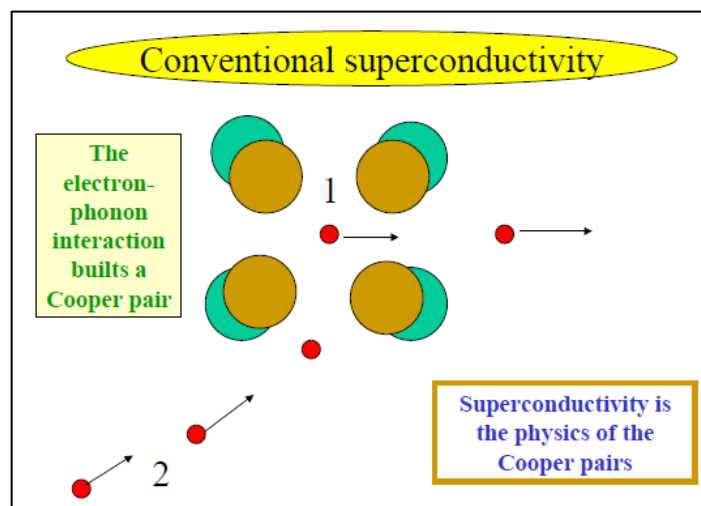


Figure 4.4: The correlation of a Cooper pair (Baquero, 2005)

The Fermi surface becomes a sphere with radius of equation (4.3). After that, states with the characteristic of $k < k_F$ will be occupied. Two electrons are brought together to this Fermi gas. They occupy space with the Pauli exclusion principle of $k > k_F$. A net attraction, U exists between two electrons when their energy goes up to certain cutoff energy, ϵ_c . Cooper also proved that even if both electrons have the state of $h > h_F$, a bound state below $2\epsilon_F$ will exist. This bound state is known as Cooper pair (Baquero, 2005).

4.3.4 Mattis-Bardeen's Formulation

To highlight the outcomes of the study, different types of methods to compute loss in circular waveguides are plotted for analysis. Yeap (2011) has developed an accurate formulation to compute loss in a circular waveguide. Since his equation has been found to agree closely with the experimental result (at frequencies below cutoff), we employ his method here in our study. To compute loss of superconducting waveguide, we substitute the complex conductivity of a superconductor into Yeap's formulation.

The results are compared by observing the trend lines of the attenuation signals. They exhibit the same characteristic which is experiencing the loss of signal as it propagates through a medium. In this project, we are interested to investigate the attenuation, skin depth, and surface resistance in both superconducting and normal circular waveguides.

Mattis and Bardeen have developed a formulation to describe the conductivity of a superconductor based on the BCS theory. The equation has been able to indicate clearly the state of transition from superconductors to normal states.

The equations for the complex conductivity by Mattis and Bardeen are shown in equation (4.4) and (4.5) below (Bardeen et al., 1957).

$$\begin{aligned} \frac{\sigma_1}{\sigma_n} &= \frac{2}{\hbar\omega} \int_{\Delta}^{\infty} [f(E) - f(E + \hbar\omega)] \frac{E^2 + \Delta^2 + \hbar\omega E}{(E^2 - \Delta^2)^{1/2} [(E + \hbar\omega)^2 - \Delta^2]^{1/2}} dE \\ &+ \frac{1}{\hbar\omega} \int_{\Delta - \hbar\omega}^{-\Delta} [1 - 2f(E + \hbar\omega)] \frac{E^2 + \Delta^2 + \hbar\omega E}{(E^2 - \Delta^2)^{1/2} [(E + \hbar\omega)^2 - \Delta^2]^{1/2}} dE \end{aligned} \quad (4.4)$$

$$\frac{\sigma_2}{\sigma_n} = \frac{1}{\hbar\omega} \int_{\Delta - \hbar\omega, -\Delta}^{\Delta} [1 - 2f(E + \hbar\omega)] \frac{E^2 + \Delta^2 + \hbar\omega E}{(E^2 - \Delta^2)^{1/2} [(E + \hbar\omega)^2 - \Delta^2]^{1/2}} dE \quad (4.5)$$

where

σ_n = the normal conductivity, and

$\Delta = \Delta(T)$ is the energy-gap parameter

The function,

$$f(E) = \frac{1}{1 + \exp(E/kT)} \quad (4.6)$$

gives the Fermi-Dirac statistics and k is the Boltzmann's constant. The first integral in equation (4.4) describes the effect of the thermally describe quasiparticles. The second integral which is (4.5) defines the generation of quasiparticles by fields with frequencies f corresponding to energies beyond the gap energy. Therefore, the second integral is zero for $\hbar\omega < 2\Delta$, where Δ depends on temperature which is obtained from equation (4.7) (Kautz, 1978).

$$\ln(\tilde{\Delta}) = -2 \int_0^{\infty} (E^2 + \tilde{\Delta}^2)^{-1/2} \left\{ 1 + \exp \left[(\pi/\gamma_E \tilde{T})(E^2 + \tilde{\Delta}^2)^{1/2} \right] \right\}^{-1} dE \quad (4.7)$$

Where, $\tilde{\Delta} = \frac{\Delta(T)}{\Delta(0)}$, $\tilde{T} = \frac{T}{T_c}$, and $\gamma_E = 1.781$ is the Euler's constant (Yeap et al., 2011).

4.3.5 Noguchi-Naruse-Sekimoto Formulation

Recently, there are researches which indicate that quasiparticle states, which are also known as intragap states, are found to exist in superconductors (Yeap et al., 2011). Therefore, Noguchi, Naruse and Sekimoto have developed a new formulation which takes into account the presence of the intragaps states. Their formulation is an extension of the Mattis-Bardeen equation. The theoretical results have been shown to agree with experimental measurements. The formulations are shown in equation (4.8)

$$\begin{aligned}
\frac{\sigma_1 - j\sigma_2}{\sigma_n} = & \\
& \frac{2}{\hbar\omega} \int_{\Delta_1}^{\infty} \frac{[f(E_r) - f(E_r + \hbar\omega)](E_r^2 + \Delta^2 + \hbar\omega E_r)}{(E_r^2 - \Delta^2)^{\frac{1}{2}}[(E_r + \hbar\omega)^2 - \Delta^2]^{\frac{1}{2}}} dE_r \\
& + \frac{1}{\hbar\omega} \int_{-\Delta_1}^{-\Delta_1 + \hbar\omega} \frac{[1 - 2f(E_r - \hbar\omega)](E_r^2 + \Delta_1^2 - \hbar\omega E_r)}{(E_r^2 - \Delta_1^2)^{\frac{1}{2}}[(E_r - \hbar\omega)^2 - \Delta_1^2]^{\frac{1}{2}}} dE_r \\
& - \frac{1}{\hbar\omega} \int_{-\Delta_2}^0 \frac{[1 - 2f(\Delta_1 + jE_i)][(\Delta_1 + jE_i)(\Delta_1^2 + jE_i - \hbar\omega) + \Delta^2]}{[(\Delta_1 + jE_i)^2 - \Delta^2]^{\frac{1}{2}}[(\Delta_1 + jE_i - \hbar\omega)^2 - \Delta^2]^{\frac{1}{2}}} dE_i \\
& + \frac{1}{\hbar\omega} \int_{-\Delta_2}^0 \frac{[1 - 2f(\Delta_1 + jE_i)][(\Delta_1 + jE_i)(\Delta_1^2 + jE_i + \hbar\omega) + \Delta^2]}{[(\Delta_1 + jE_i)^2 - \Delta^2]^{\frac{1}{2}}[(\Delta_1 + jE_i + \hbar\omega)^2 - \Delta^2]^{\frac{1}{2}}} dE_i \tag{4.8}
\end{aligned}$$

where

Δ_1 = Real gap energy

Δ_2 = Imaginary gap energy

E_r = Real part of the complex quasiparticle excitation energy

E_i = Imaginary part of the complex quasiparticle excitation energy

\hbar = Reduced Planck's constant

ω = Angular frequency

4.3.6 TE and TM Modes of Circular Waveguides

By solving the Helmholtz equation, the longitudinal electric and magnetic field E_z and H_z , propagating in a circular waveguide, as shown in Figure 4.5 can be derived. Next, the field equations which are show in equation (4.9) and (4.10) are obtained using the method of separation of variables.

$$H_z = C_n' J_n(hr) \sin n \phi, \quad (4.9)$$

$$E_z = C_n J_n(hr) \cos n \phi, \quad (4.10)$$

where

C_n and C_n' denote the coefficients of the longitudinal fields in equation (4.11)

$$h = \sqrt{k^2 - k_z^2}, \quad (4.11)$$

where

k = wavenumber in free space,

k_z = propagation constant,

r = the radial distance,

$J_n(hr)$ = Bessel function of the first kind,

$J_n'(hr)$ = its derivative, and

n = the order of the Bessel function

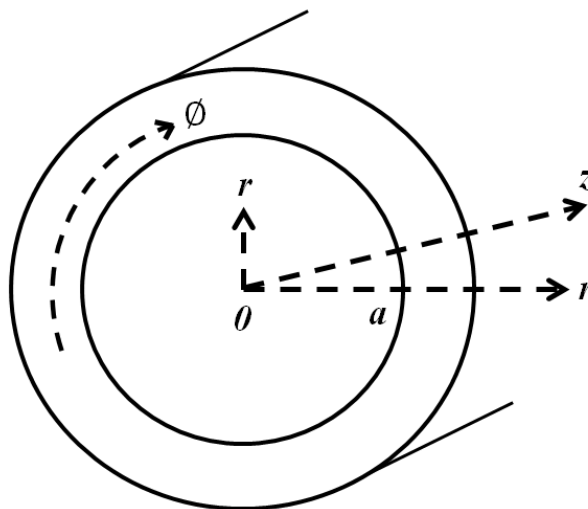


Figure 4.5: A circular waveguide

All field components consist of the wave factor in the form of $\exp[j(\omega t - k_z z)]$, where t represents the time and ω is the angular frequency. Therefore, the wave factor is omitted in the following derivations.

The propagation constant k_z is a complex variable which constitutes a phase constant β_z and an attenuation constant α_z , as shown as equation (4.12) below.

$$k_z = \beta_z - j\alpha_z \quad (4.12)$$

By substituting (4.9) and (4.10) into Maxwell's source-free curl equations and expressing the transverse field components in terms of E_z and H_z , equations (4.13) and (4.14) are obtained.

$$E_\phi = \frac{1}{h^2} \left[\frac{jnk_z}{r} C_n J_n(hr) \sin n\phi + j\omega\mu h C_n' J_n'(hr) \cos n\phi \right] \quad (4.13)$$

$$H_\phi = -\frac{1}{h^2} \left[\frac{jnk_z}{r} C_n' J_n(hr) \cos n\phi + j\omega\epsilon h C_n J_n'(hr) \cos n\phi \right] \quad (4.14)$$

At the wall of waveguide, the tangential electric and magnetic fields are related through a surface impedance Z_s which is shown in equation (4.15).

$$E_t = -Z_s(a_n \times H_t) \quad (4.15)$$

At the boundary of the wall with radius $r = a$, $Z_s = \frac{E_\phi}{H_z} = -\frac{E_z}{H_\phi} = \sqrt{\frac{\mu_w}{\epsilon_w}}$. By substituting equations (4.9), (4.10), (4.13), and (4.14) into (4.15), and solves the determinants of coefficients C_n and C_n' , the transcendental equations in (4.16) and (4.17) are obtained. Equation (4.16) is TE modes while (4.17) is TM modes.

$$\left[jh^2 \sqrt{\frac{\mu_w}{\epsilon_w}} + \omega\mu h \frac{J_n'(ha)}{J_n(ha)} \right] \left[jh^2 \sqrt{\frac{\epsilon_w}{\mu_w}} + \omega\epsilon h \frac{J_n'(ha)}{J_n(ha)} \right] = \left[\frac{nk_z}{a} \right]^2 \quad (4.16)$$

$$\left[jh^2 \sqrt{\frac{\mu_c}{\epsilon_c}} \frac{J_n(u)}{J_n(u)'} + \omega\mu h \right] \left[jh^2 \sqrt{\frac{\mu_c}{\epsilon_c}} \frac{J_n(u)}{J_n(u)'} + \omega\epsilon h \right] = \left[\frac{nk_z}{a} \frac{J_n(u)}{J_n(u)'} \right]^2 \quad (4.17)$$

4.4 Results and Discussion

Cutoff frequency, f_c in a waveguide is the point of frequency where the waves begin to transmit in the direction of field. In Figure 4.6 shows the attenuation of the dominant TE_{11} mode in circular waveguides below f_c .

From the graph, it can be observed that the attenuation of superconducting waveguides and normal waveguides below cutoff agree closely with each other. They exhibit approximately the same characteristic, i.e. they decrease sharply as frequency increases. The loss computed using Noguchi-Naruse-Sekimoto's equation in (4.8) and Mattis-Bardeen's equations in (4.4) and (4.5) agree very closely to each other as well. Since both approaches are developed from the BCS theories, the results shows that they are in consistence with each other.

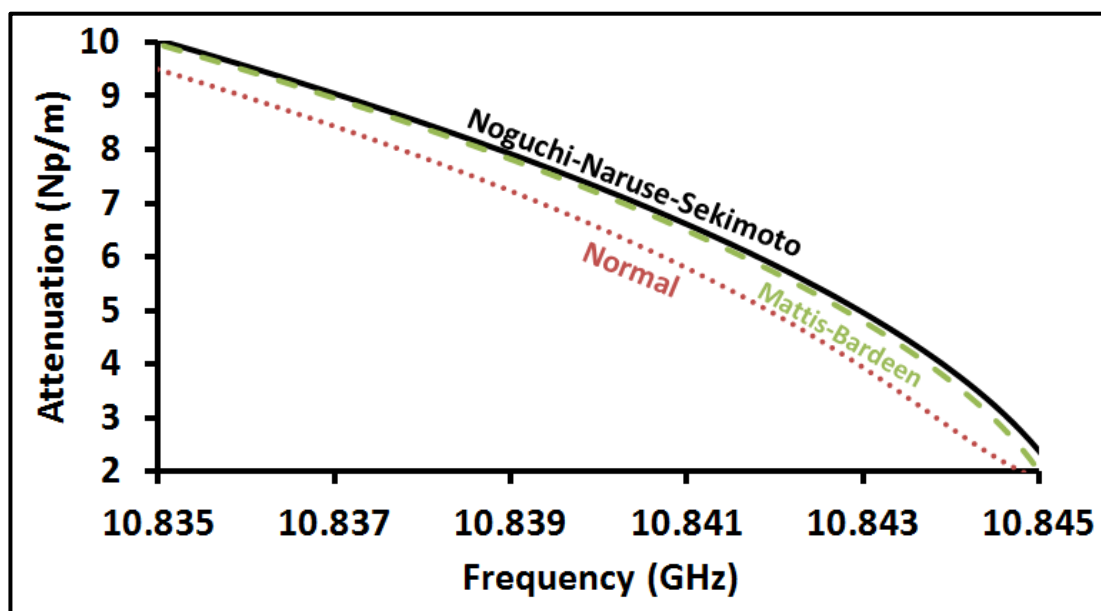


Figure 4.6: Attenuation before cutoff frequency, f_c

As can be observed in Figure 4.7, when frequency increases until it exceeds the cutoff frequency, the attenuation in superconducting waveguides is obviously lower than in normal conducting waveguides. In fact, the attenuation computed using Mattis-Bardeen's equations is close to zero. This is because according to Mattis and Bardeen, the presence of quasiparticles is nearly negligible at f below the gap frequency f_g . Since the collision of quasiparticles results in energy loss, when the quasiparticles are absent, Mattis and Bardeen's equation expects no loss in the waveguide. However, in recent research related to the properties of superconducting waveguides, Niobium shows measurable losses (Kushino et al., 2013; Ciovati et al., 2010).

The measurable loss of the research proves that the loss in superconducting waveguides is measurable at f below f_g although its loss is expected to be very low. Therefore, the attenuation trend line obtained by using Noguchi-Naruse-Sekimoto's complex conductivity is more practical compared to Mattis-Bardeen. The reason is, Noguchi-Naruse-Sekimoto's complex conductivity involves the existence of the intragap states but Mattis-Bardeen's has not.

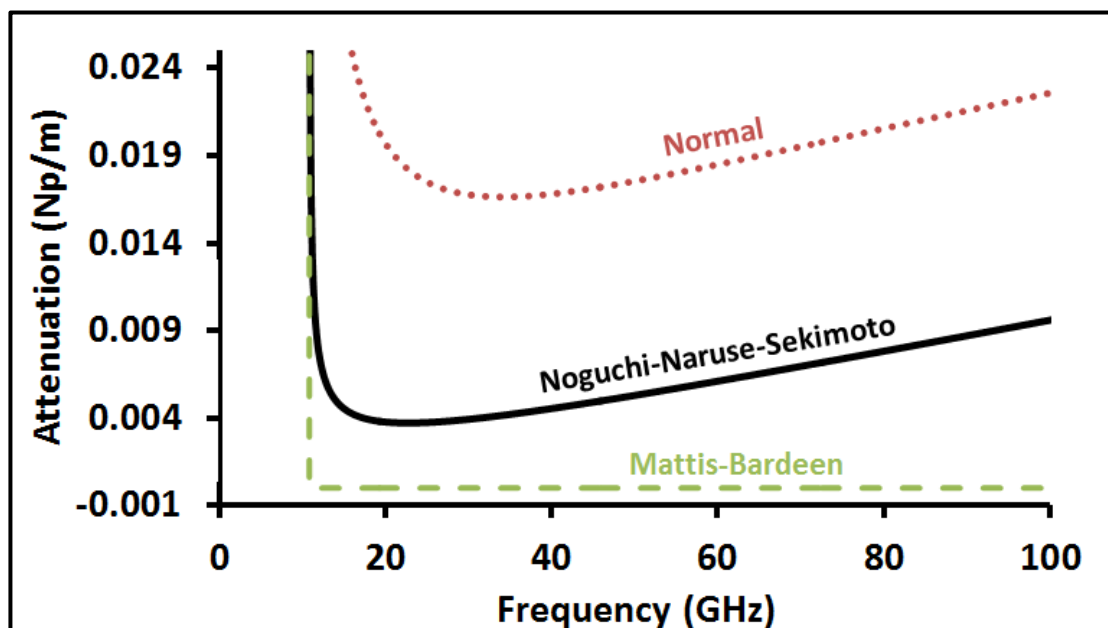


Figure 4.7: Attenuation from cutoff to millimeter wave frequencies

From Figure 4.8, we can observe that the attenuation of circular waveguides from cutoff to terahertz frequencies. The attenuation using Mattis-Bardeen complex conductivity remains zero before the gap frequency, f_g . From this graph, it is obvious that attenuation using Noguchi-Naruse-Sekimoto's formulation is higher than Mattis-Bardeen's formulation but is lower than normal conducting waveguides in the beginning stage. The high loss characteristic of Noguchi-Naruse-Sekimoto's attenuation is due to the additional loss using equation (4.8) which is affected by the quasiparticles at the intragap states. Furthermore, the loss in superconducting waveguide is reduced when the temperature T decreases further from critical temperature T_c .

On the contrary, the imaginary part of the gap energy was ignored in Mattis and Bardeen's equations, as seen in equation (4.4). Therefore, the attenuation before the gap frequency was neglected as seen as Figure 4.8. This proves that intragap states play an important role because it is able to predict the small but measurable loss found in superconducting waveguides.

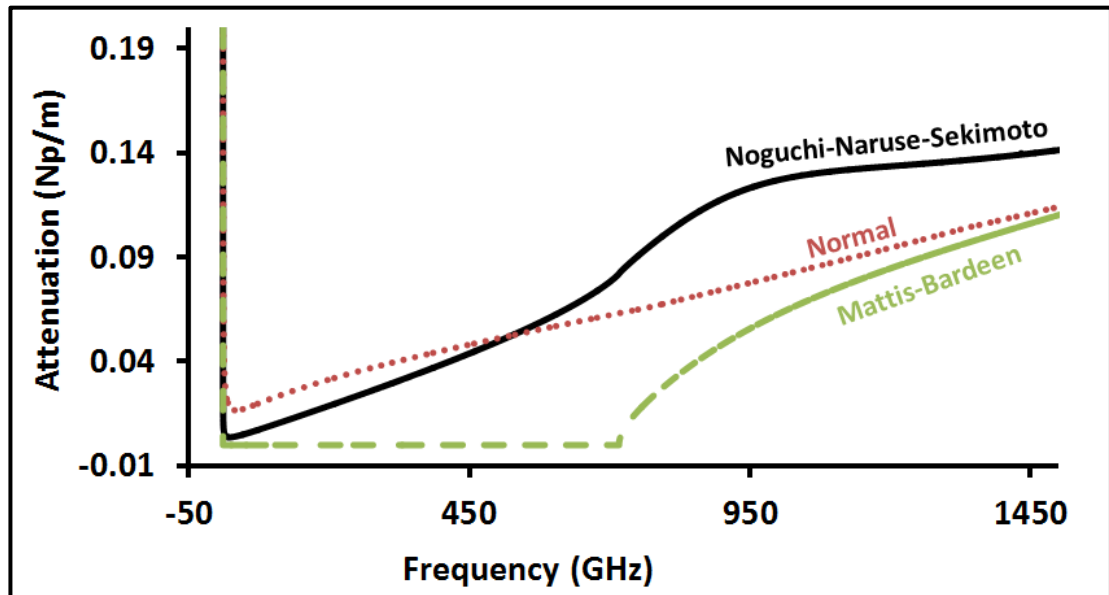


Figure 4.8: Attenuation from cutoff to THz frequencies

Figure 4.9 shows the close view of both methods of complex conductivity at the vicinity of gap frequency f_g . The observation shows that when frequency f exceeds the gap frequency f_g which is approximately 716.45 GHz, the attenuation of waveguides begin to increase sharply. Furthermore, as we can observe in Figure 4.8, the attenuation in superconducting waveguides tends to surpass the normal waveguides which is operating at room temperature.

This fact is caused by the increase of quasiparticles triggered by the gap frequency at 716.45GHz. As the photon energy $\hbar\omega$ surpasses the gap energy at $2\Delta(4.2\text{K})$, Cooper pairs are broken into quasiparticles. Consequently, the higher loss at frequencies above gap frequency f_g is affected by the random collision of increasing number of quasiparticles with the lattice structure.

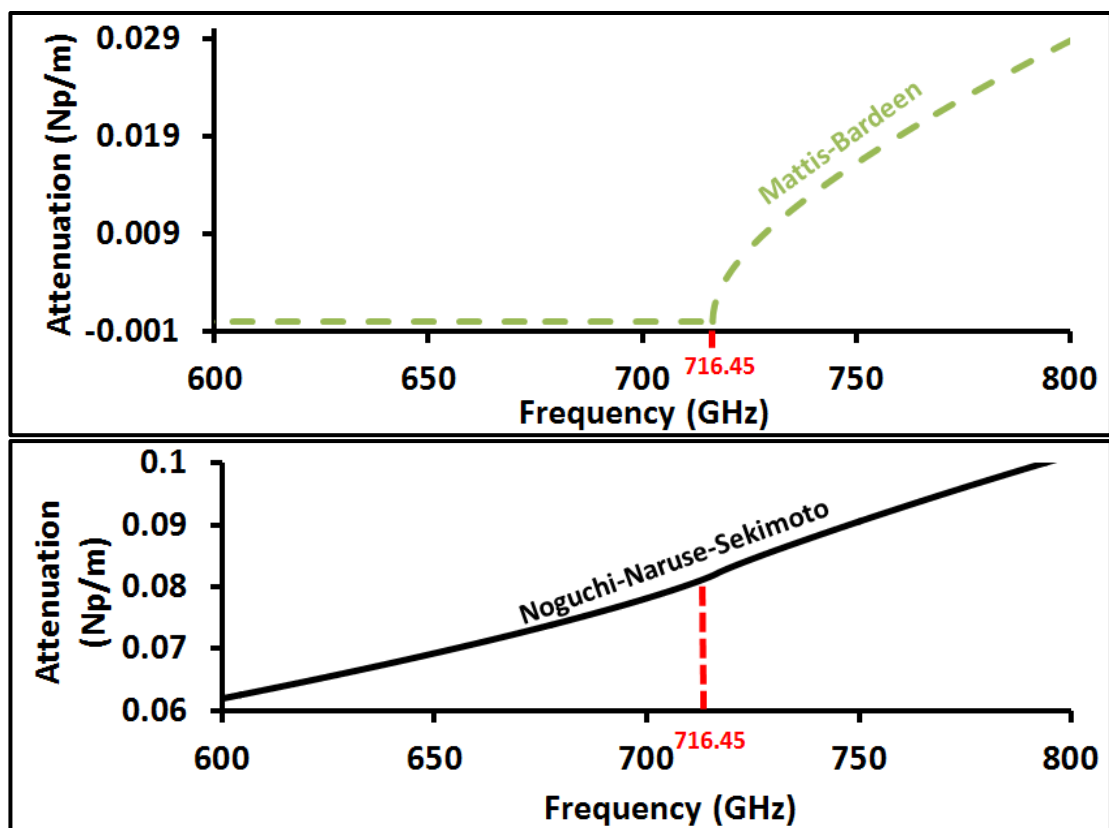


Figure 4.9: Attenuation in a superconducting Nb waveguide at the vicinity of gap frequency

4.4.1 Skin Depth

Skin depth is a measure of how closely electric current flows along the surface of a material. Skin depth is also known as depth of penetration. It is also a measure of the depth to which an electromagnetic wave can penetrate the medium (Raju, 2006). The ohmic power loss in the waveguides is directly proportional to the surface resistance R_s and current induced by the magnetic field penetration in the wall. The skin depth δ is given in equation (4.18) below.

$$\delta = \sqrt{\frac{2}{\omega\mu\sigma}} \quad (4.18)$$

where

μ = permeability of Niobium (Nb)

σ = complex conductivity of Niobium (Nb)

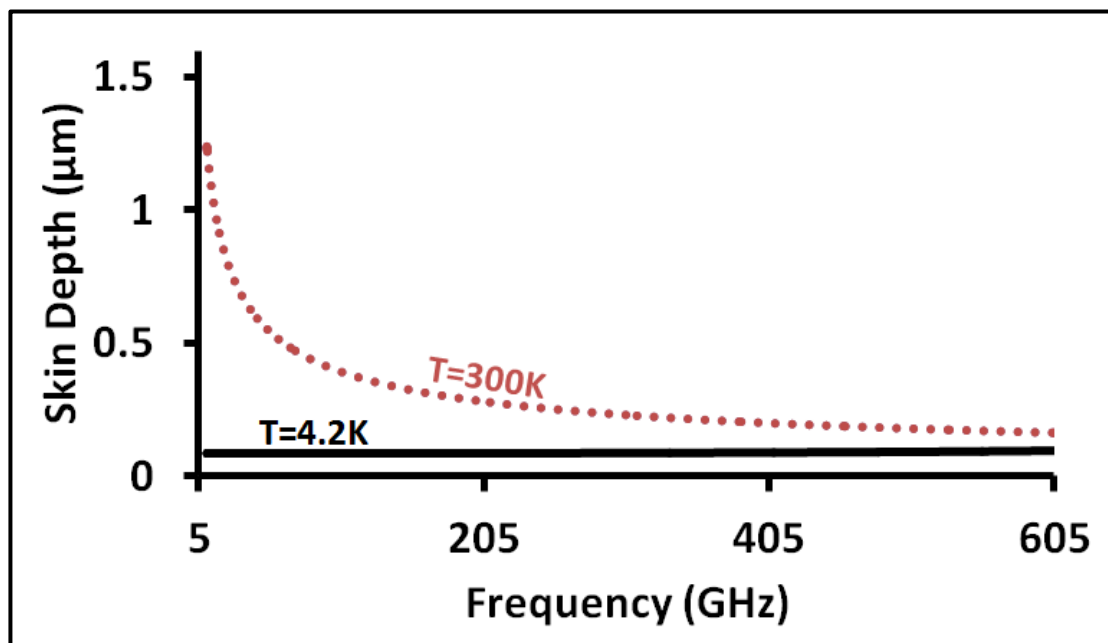


Figure 4.10: Comparisons between the skin depth of Nb in superconducting and normal states, with f below f_g

Figure 4.10 and 4.11 shows the comparisons between skin depth δ of Nb at different frequency ranges. As we can observe in Figure 4.10, the skin depth δ using superconducting waveguides ($T=4.2\text{K}$) is much smaller than normal conducting waveguides ($T=300\text{K}$) before the gap frequency f_g . For this case, the field penetration in the normal state is larger than in superconducting state. However, when the frequency exceeds the gap frequency f_g , the superconducting Nb becomes much higher than the normal conducting state as we can see in Figure 4.11.

The attenuation and skin depth of waveguides have a close relationship between each other. By investigating the graphs of attenuation in Figure 4.8 and 4.11, we can examine that the skin depth and attenuation are relatively low before the gap frequency f_g . However, there is a sudden increase of attenuation and skin depth after surpassing the gap frequency f_g . This phenomenon suggests that, the skin depth effect is one of the factors which affect the level of attenuation in waveguides. Apparently, this also explains why the loss of superconducting Nb is lower. As according to Poynting's theorem, the lower skin depth means there is low power flow per unit area through the surface of waveguides (Bakshi & Bakshi, 2008).

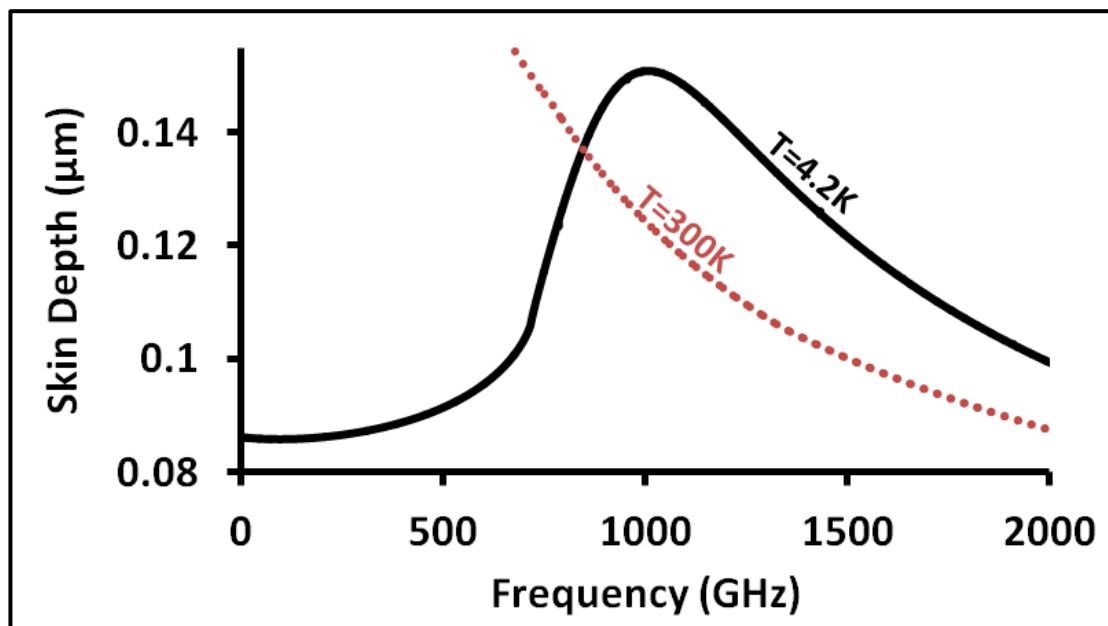


Figure 4.11: Comparisons between the skin depth of Nb in superconducting and normal states, with $f = 0$ GHz to $f = 2000$ GHz

4.4.2 Surface Resistance

The surface resistance is the ohmic losses in the form of radiation in the outer medium of waveguide. The reflection upon the wall is caused by surface resistance. There have been researches about surface resistances of circular waveguides at millimeter wavelength since 1976 (Hatano & Nihei, 1976). The surface resistance R_s of waveguides can be obtained by substituting the values of complex conductivity into the real part of Z_s of circular waveguides which stated in equation (4.19). As shown in Figure 4.12, R_s of superconducting Nb at 4.2K increases at a higher rate than at room temperature which is a normal conducting waveguides.

$$Z_s = \sqrt{\frac{\mu_\omega}{\varepsilon_\omega}} \quad (4.19)$$

where

μ_ω = Permeability of the wall material of waveguides

ε_ω = Permittivity of the wall material of waveguides

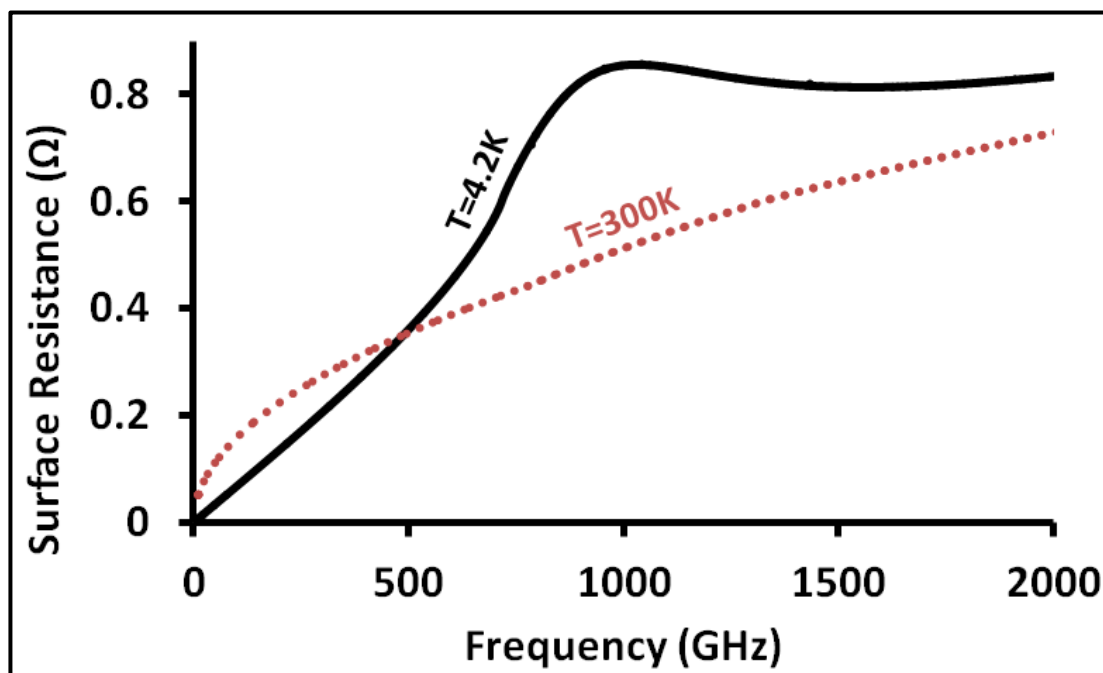


Figure 4.12: The surface resistance of Nb in both normal and superconducting state

However, R_s of Nb at 4.2K which is the superconducting waveguides exceeds the normal Nb when the frequency increases above approximately 500GHz. The surface resistance of superconductor was derived as in equation (4.20) using two fluid model (Duzer & Turner, 1981).

$$R_s = \frac{\omega^2 \mu^2 \lambda_L^3 n_n \sigma_n}{2} \quad (4.20)$$

where

n_n = the number density of the quasiparticles

As can be observed, the surface resistance R_s for superconductors increases as the square root of the frequency, while the R_s for normal conductors only increases proportional to the square root. Therefore, the higher loss which occurs in a superconducting waveguide in Figure 4.8 can be attributed to the higher surface resistance and greater penetration depth for frequencies above gap frequency.

According to Figure 4.8, when the frequency is below the gap frequency f_g , the surface resistance increases in direct proportion with frequency. However, as the frequency goes above gap frequency f_g , the surface resistance rises sharply. This phenomenon happens due to the fact that Cooper pairs start to separate into quasiparticles. Random collision occurs due to the presence of more quasiparticles. Thus, the lattice structure of the conductor occurs and causes a higher surface resistance.

CHAPTER 5

CONCLUSION AND RECOMMENDATIONS

5.1 Conclusion

The calculation of attenuation in waveguides plays an important role in today's technology. Minimization of loss during the propagation of signal is also a vital step to determine the quality of the heterodyne receiver in a radio telescope. The attenuation was successfully calculated using the extended theory of Mattis-Bardeen by Noguchi-Naruse-Sekimoto's method.

In the analysis of reflector antennas, the result suggests that hybrid coupling of Method of Moments (MoM) and Physical Optics (PO) yield accurate and consistent result compared to the non-coupling method of antenna design. The configuration of the ALMA Cassegrain antenna was applied in the reflector design to detect signal with low frequency such as 10 GHz. In this part, the radiation pattern at the subreflector suggests that the configuration may be applicable for lower frequency at 10 GHz.

In superconducting waveguides, the attenuations were computed using different approaches i.e. using Mattis-Bardeen's and Noguchi-Naruse-Sekimoto's equations. Furthermore, the comparison of attenuation between superconducting and normal waveguides is also performed. The results show that by applying Noguchi-Naruse-Sekimoto's formulation, the presence of quasiparticles in the intragap states and their effect on the attenuation and surface resistance of a superconducting waveguide can be described effectively. One important study of this

project that the loss obtained by using Noguchi-Naruse-Sekimoto's formulation above gap frequency f_g is higher than the loss produced by using Mattis-Bardeen's formulation.

In short, the objectives of this project are successfully achieved. We were able to compare and analyse the loss in superconducting waveguides using different approaches. In addition, the performance of reflector antennas in radio telescopes was successfully simulated using FEKO software.

5.2 Recommendation

The project was carried out successfully since superconducting waveguides and reflector antennas generate reasonably good result. In this section, we give several recommendations to improve the performance of a radio telescope and the accuracy of the results.

5.2.1 Superconducting Waveguides

In this project, circular waveguide was implemented to calculate the attenuation of wave propagation. In the future, it would be recommended to try new structure of waveguide using Noguchi-Naruse-Sekimoto's extended theory of Mattis-Bardeen. The other wave guiding structures can be applied such as coplanar waveguides and superconducting microstrips.

In addition, real-life experiments on physical superconducting structures may be applied to validate the characteristic of superconducting waveguides in real life. By comparing results computed from existing theories with those found from measurements, the rate of accuracy can be obtained.

5.2.2 Reflector Antennas

Although our preliminary result shows that the main lobe is considerably higher than side lobes, further analysis is still required in order to verify the applicability of the ALMA reflector antenna on a 10 GHz signal. We suggest to investigate the aperture efficiency, contours of the beam profiles, beam efficiency and taper and spillover loss of the reflector antennas. Optimization can be performed to determine the optimum configuration for the reflector antenna for 10 GHz.

REFERENCES

- Akalin, T., Treizebre, A. & Bocquet, B., 2006. Single Transmission Lines at Terahertz Frequencies. *IEEE Transactions on Microwave Theory and Techniques*, 54(6), pp.2762-67.
- Bakshi, U.A. & Bakshi, A.V., 2008. *Electromagnetic Waves and Transmission Lines*. 5th ed. India: Technical Publications.
- Balanis, C.A., 2005. *Antenna Theory*. 3rd ed. New Jersey: John Wiley & Sons.
- Baquero, R., 2005. *Brief Introduction to Superconductivity*. Cinvestav: Departamento de Fisica.
- Bardeen, J., Cooper, L.N. & Schrieffer, J.R., 1957. Theory of Superconductivity. *The Physical Review*, 108(5), pp.1175-204.
- C. Y. Tham, S.W.a.G.Y., 2009. *Optimisation of ALMA Feed Optics*. United Kingdom: Cavendish Laboratory, University of Cambridge.
- Ciovati, G., Myneni, G. & Stevie, F., 2010. High field Q slope and the baking effect: review of recent experimental results and new data on Nb heat treatments. *Phys. Rev. ST Accel. Beams*, 13, pp.1-22.
- David, B.L., 1996. Fortran: A Modern Standard Programming Language For Parallel Scalable High Performance Technical Computing. In *Internal Conference on Parallel Processing Workshop*. Maynard, 1996. Digital Equipment Corporation.
- Duzer, T.V. & Turner, C.W., 1981. *Principles of Superconductive Devices and Circuits*. 1st ed. New York: US: Elsevier.

- Goldsmith, P.F., 1998. *Quasioptical system - Gaussian beams quasioptical propagation and application*. New York: IEEE Press Marketing.
- Hatano, S. & Nihei, F., 1976. Measurement of Surface Resistance in Oversized Circular Waveguide at Millimeter Wavelengths. *IEEE Transactions on Microwaves Theory and Techniques*, pp.886-87.
- Hu, B., Xu, X. & He, M., 2009. More accurate Hybrid PO-MOM analysis for an electrically large antenna-radome structure. *Progress in Electromagnetics Research, PIER*, 92, pp.255-65.
- Jacob, W.M.B., 1992. Design Philosophy and Technology Aspects of Submillimeter Wavelength Radio Telescopes. *IEEE MTT-S Digest*, pp.1251-54.
- John, F.W., Roman, S. & Douglas, R.D., 1988. Propagation model for ultrafast signals on superconducting dispersive striplines. *IEEE Transactions on Microwave Theory and Techniques*, 36(2), pp.277-85.
- Joint ALMA Observatory and ESO, 2015. *RADIO ASTRONOMY MANUAL ALMA at School*. Garching bei München: ALMA (ESO/NAOJ/NRAO).
- Kato, Y. & Miyagi, M., 1992. Modes and Attenuation Constants in Circular Hollow Waveguides with Small Core Diameters for the Infrared. *IEEE Transactions on Microwave Theory and Techniques*, 40(4), pp.679-85.
- Kautz, R.L., 1978. Picosecond pulses on superconducting striplines. *Journal of Applied Physics*, pp.308-14.
- Kikuchi, K., Yamada, T. & Kohjiro, S., 2011. Development of Superconductor-Insulator-Superconductor (SIS) Terahertz Receiver With Mechanical and Thermal Vibration-Reduced Cryocooler. *IEEE Transactions on Applied Superconductivity*, 21(3), pp.649-53.

- Kopnin, N.B., 2009. *Introduction to The Theory of Superconductivity*. Finland: Cryocourse.
- Kurokawa, K., 1962. Electromagnetic Waves in Waveguides with Wall Impedance. *IRE Transactions on Microwave Theory and Techniques*, pp.314-20.
- Kushino, A., Teranishi, Y. & Kasai, S., 2013. Low temperature properties of a superconducting niobium coaxial cable. *J. Superconduct. Novel Magn.*, 26, pp.2085-88.
- Leal-Sevillano, C.A., Ruiz-Cruz, A. & Montejo-Garai, J.R., 2011. Field Propagation in Circular Hollow Waveguides With Non-Ideal Metallic Conductors From Microwaves to Terahertz Frequencies. *IEEE Transaction on Microwave Theory and Techniques*, 59(12), pp.3013-22.
- Marcuvitz, N., 1951. *Waveguide Handbook*. New York: McGraw Hill.
- Michael, S., 2005. Terahertz technology: devices and applications. *IEEE*, pp.13-21.
- Michael, A.H. & Alan, P., 1980. A Static Analysis of the NAG Library. *IEEE Transactions on Software Engineering* , SE-6(4), pp.329-33.
- Raju, G.S.N., 2006. *Electromagnetic Fied Theory and Transmission Lines*. India: Pearson.
- Stratton, J.A., 1941. *Electromagnetic Theory. In: Boundary-Value Problems*. 1st ed. New York: McGraw-Hill.
- Tham, C.Y. & Withington, S., 2003. *The Atacama Large Millimeter Array Receiver Optics Design Electromagnetic Analysis*. United Kingdom: Cavendish Laboratory University of Cambridge.
- Tham, C.Y., Withington, S. & Yassin, G., 2009. *Optimisation of ALMA Feed Optics*. United Kingdom: Cavendish Laboratory, University of Cambridge.

- Tham, C.Y., Yassin, G. & Carter, M., 2007. Analysis techniques for the optics in millimetre/submillimetre wave radio telescope receivers. *JURNAL FIZIK MALAYSIA*, 28(1&2), pp.49-54.
- Yassin, G., Jung, G. & Dikovsky, V., 2001. Investigation of microwave propagation in high-temperature superconducting waveguides. *IEEE Microwave and Wireless Component Letters*, 11, pp.413-15.
- Yassin, G., Tham, C.Y. & Withington, Y., 2003. Propagation in lossy and superconducting cylindrical waveguides. *14th International Symposium on Space Terahertz Technology*, pp.22-24.
- Yeap, K.H., Nisar, H., Loh, S.H. & Humaira, N., 2013. Analysis of Probes in a Rectangular Waveguide. *Frequenz Journal of RF-Engineering and Telecommunications* , 67(5-6), pp.145-54.
- Yeap, K.H., Tham, C.Y. & Yassin, G., 2011. Attenuation in Rectangular Waveguides with Finite Conductivity Walls. *Radioengineering Journal*, 20(2), pp.472-78.
- Yeap, K.H., Tham, C.Y. & Yeong, K.C., 2009. A simple method for calculating attenuation in waveguides. *Frequenz Journal of RF-Engineering and Telecommunications*, 63, pp.236-40.
- Yeap, K.H., Tham, C.Y. & Yeong, K.C., 2010. Wave Propagation in Lossy and Superconducting Circular Waveguides. *Radioengineering*, 19(2), pp.320-25.
- Yeap, K.H., Yeong, K.C. & Hirasawa, K., 2015. Attenuation in Superconducting Rectangular Waveguides. *Frequenz* , 69(3-4), pp.111-17.

